Time- and frequency-domain models for Smith-Purcell radiation from a two-dimensional charge moving above a finite length grating

Amit S. Kesar,* Mark Hess,† Stephen E. Korbly, and Richard J. Temkin
Plasma Science and Fusion Center, Massachusetts Institute of Technology, Cambridge, Massachusetts 02139, USA
(Received 23 July 2004; revised manuscript received 22 September 2004; published 11 January 2005)

Smith-Purcell radiation (SPR), formed by an electron beam traveling above a grating, is a very promising source of coherent radiation from the THz to the optical regime. We present two theoretical calculations of the SPR from a two-dimensional bunch of relativistic electrons passing above a grating of finite length. The first calculation uses the finite-difference time-domain approach with the total-field/scattered-field procedure for fields incident on the grating. This calculation allows good physical insight into the radiation process and also allows arbitrary geometries to be treated. The second calculation uses an electric-field integral equation method. Good agreement is obtained between these two calculations. The results of these theoretical calculations are then compared with a theoretical formalism based on an infinite-length grating. The latter formalism allows periodic boundary conditions to be rigorously applied. For gratings with less than ~50 periods, a significant error in the strength of the radiated field is introduced by the infinite-grating approximation. It is shown that this error disappears asymptotically as the number of periods increases. The Wood-Rayleigh anomalies, predicted in the infinite-grating approximation, were not seen in our finite-grating calculations. The SPR resonance condition is the same in all three formalisms. Numerical examples are presented for an ~18 MeV, 50 nC/m, 200 μm bunch traveling 0.6 mm above a ten-period echelle grating having a 2.1-mm periodicity.

DOI: 10.1103/PhysRevE.71.016501 PACS number(s): 41.60.−m, 02.70.Bf, 42.25.Fx, 42.79.Dj

I. INTRODUCTION

Smith-Purcell radiation (SPR) [1] is typically formed by an electron bunch traveling at a velocity v_x and height $b_{\min}$ above a periodic grating, as shown in Fig. 1. A theoretical analysis of SPR was derived by Toraldo Di Francia [2] in which the electromagnetic (EM) radiation, generalized as Čerenkov radiation, is caused by diffraction of evanescent waves from the grating. These evanescent waves are generated by a charge traveling in free space. Integral equation methods are used to rigorously solve a wide variety of EM problems in the frequency domain. The rigorous solution by van den Berg of the SPR emitted by a line [3] or a point [4] charge moving parallel to an infinitely long grating is obtained by solving an integral equation having a periodic Green's function. Based on the evanescent-wave approach by Toraldo Di Francia and the exact integral method by van den Berg, Haeberlé *et al.* calculated the SPR for a point charge with energies of 1–100 MeV [5]. Transition radiation is also calculated by using integral equations in various papers such as [6,7]. An induced surface current model was developed by Walsh *et al.* for SPR from a strip grating [8], and Brownell *et al.* generalized it for an arbitrary grating profile [9]. This model is based on the image-charge approximation; however, a two-dimensional (2D) model for arbitrary grating profiles has not been published.

In common with all of the above models is the agreement on the coherence factor from a finite bunch length and the agreement on the SPR resonance condition. The latter is given by

$$n\lambda = D_g(\beta^{-1} - \sin\theta), \tag{1}$$

where the nth radiation order of the SPR wavelength, λ, in the xz plane, is a function of the spatial angle θ, the relativistic bunch velocity $\beta = v_x/c = (1-\gamma^{-2})^{1/2}$, and the grating period D_g, as illustrated in Fig. 1. The diffracted radiated pulse from the grating is coherent for wavelengths larger than, or on the order of, the bunch length [10] and the number of periods in the pulse is equal to the number of grating grooves.

The SPR due to gratings having small number of periods was studied experimentally by Burdette and Hughes [11]. The radiation bandwidth from these gratings was found to be dependent on the number of grating grooves. A comparison of the radiated energy to theoretical models has been done in many recent SPR experiments having various grating densities and lengths. A good agreement for the relative dependence on the bunch height above the grating was obtained. A

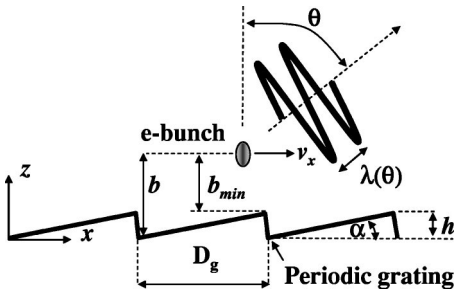

FIG. 1. The SPR scheme. An electron bunch is traveling at an axial velocity v_x above an echelle grating of period D_g.

*Corresponding author. Electronic address: a_kesar@mit.edu
†Present address: Physics Department, Indiana University, Bloomington, IN 47405, USA.

TABLE I. Grating and bunch parameters in few Smith-Purcell experiments.

Experiment	L(mm)	N_g	$b_{\min}$(mm)	γ
Mainz Microtron [15]	25	30000	0.1	1674
RRI, Kyoto [12]	120	60	2.5	295
MIT [20]	100	47	0.5	30
Frascati FEL [13]	100	40	1	4.52

comparison of the absolute energy at various observation angles with the theoretical prediction is of great interest. Some data have been obtained, but the measurement is very difficult and results are limited [12–15].

The radiated energy is proportional to the grating length L. While in experimental setups the grating length is restricted by the bunch emittance and cross section and by the size of the output optics inside the vacuum chamber, the rigorous analytical solution by van den Berg [3,4] assumes an infinitely long grating. Thus, the measured radiated energy may deviate with respect to theoretical predictions based on van den Berg's model, and therefore, rigorous models taking into account a finite grating length are essential for calculating the output of practical SPR experiments.

Under van den Berg's infinitely long grating assumption the radiated energy per groove equals the work done on the bunch along a groove length. Operating a SPR experiment in the van den Berg regime would require that $N_g \gtrsim 1000$ to provide a $\sim 10\%$ accuracy, where N_g is the number of grating grooves. This requirement could be qualitatively understood by comparing the ratio of a periodic Green's function which is based on a summation over an infinite number of grooves and a Green's function truncated at N_g [16]. This issue is discussed in detail in Sec. IV of this paper.

Grating and bunch parameters in a few SPR experiments are presented in Table I. In this table, only the grating in Ref. [15] fulfills this requirement. Thus, a model taking into account a finite grating length is necessary for most experiments to accurately predict the radiated intensity.

In this paper, we report the first calculation of SPR using a finite-difference time-domain (FDTD) formalism. The FDTD method is a powerful tool for calculating the EM fields for a wide range of applications such as antennas, high-speed electronic circuits, periodic and photonic bandgap structures, and optical resonators [17]. An analysis of Čerenkov radiation in photonic crystals was confirmed by FDTD simulation using a pointlike current density [18].

The diffraction of short pulses from a finite-size object could be applied to SPR setups due to the broad spectrum diffracted by the incident free-space bunch wake. Thus, the physics of the diffracted fields by the finite grating length is taken into account in detail. The FDTD technique is easily adaptable to arbitrary grating geometries and can be used to optimize the SPR and estimate the bunch length [19,20]. In addition, it provides an intuitive understanding of the SPR physics by studying its temporal behavior.

The objectives of this paper are to (a) obtain a time domain (FDTD) model for calculating the SPR emitted from a finite length grating by a 2D bunch, (b) obtain a frequency-domain electric-field integral equation (EFIE) model capable of (i) benchmarking the time-domain results for a finite length grating and (ii) benchmarking van den Berg's model [3] for the infinitely long grating assumption, and (c) determine the asymptotic convergence of the radiated energy per groove by an extended length grating to van den Berg's solution.

II. FDTD FORMULATION

An FDTD formulation is presented in order to study the temporal behavior of the SPR. In the 2D case shown in Fig. 1, an electron bunch infinite in the y direction is traveling at an average height $b_{\min}=b-h$ and velocity $\hat{x}v_x$ above a grating, where h is the groove height. The bunch free-space evanescent waves (wake fields) are TE_y polarized [2]; thus, the incident components obtained by the Lorentz transform of its electrostatic field are H_y^{inc}, E_z^{inc}, and E_x^{inc}.

Central differencing of the TE_y Maxwell equations using Yee's algorithm [21] results (with minor modifications) in the FDTD equations [17]

$$H_y|_{j+1/2,k+1/2}^{n+1/2} = H_y|_{j+1/2,k+1/2}^{n-1/2} - \frac{\Delta_t}{\mu_0 \Delta_z}\left(E_x|_{j+1,k+1/2}^{n} - E_x|_{j,k+1/2}^{n}\right) + \frac{\Delta_t}{\mu_0 \Delta_x}\left(E_z|_{j+1/2,k+1}^{n} - E_z|_{j+1/2,k}^{n}\right), \tag{2a}$$

$$E_z|_{j+1/2,k}^{n+1} = E_z|_{j+1/2,k}^{n} + \frac{\Delta_t}{\epsilon_0 \Delta_x}\left(H_y|_{j+1/2,k+1/2}^{n+1/2} - H_y|_{j+1/2,k-1/2}^{n+1/2}\right), \tag{2b}$$

$$E_x|_{j,k+1/2}^{n+1} = E_x|_{j,k+1/2}^{n} - \frac{\Delta_t}{\epsilon_0 \Delta_z}\left(H_y|_{j+1/2,k+1/2}^{n+1/2} - H_y|_{j-1/2,k+1/2}^{n+1/2}\right), \tag{2c}$$

where μ_0 and ϵ_0 are the free-space permeability and permitivity, respectively. The subscripts k and j are the spatial indices in the x and z coordinates, respectively, and the superscript n is the temporal index. The spatial resolution in the x and z coordinates is determined by Δ_x and Δ_z where $x=k\Delta_x$ and $z=j\Delta_z$. Similarly $t=n\Delta_t$ where Δ_t determines the time step. To ensure a stable solution the FDTD stability factor $\xi^2=(c\Delta_t)^2(\Delta_x^{-2}+\Delta_z^{-2})$ should be <1.

In order to calculate the diffracted fields due to the 2D bunch, we assumed that the energy lost by the charge is negligible compared to the charge initial energy, and thus a particle-in-cell computation taking into account trajectory changes is not required. This assumption can be checked at the end of the calculation by comparing the radiated energy to the initial electron bunch energy. The ratio is found to be negligible in all cases of interest. Therefore, we took advantage of the fact that the bunch wake could be represented as a set of evanescent plane waves [2] and used the total-field/scattered-field (TF/SF) technique [17] to simulate the free-space wake as the source fields incident on the grating,

$$\mathbf{E}^{\mathrm{inc}}(x,z,t) = \frac{q\gamma}{2\pi\epsilon_0}\int_{x_0}\int_{z_0}\frac{\hat{z}(z-z_0)+\hat{x}(x-x_0-v_xt)}{(z-z_0)^2+\gamma^2(x-x_0-v_xt)^2} \times f(x_0,z_0)dz_0dx_0, \tag{3a}$$

$$\mathbf{H}^{\mathrm{inc}}(x,z,t) = \frac{q\gamma v_x}{2\pi}\int_{x_0}\int_{z_0}\frac{-\hat{y}(z-z_0)}{(z-z_0)^2+\gamma^2(x-x_0-v_xt)^2} \times f(x_0,z_0)dz_0dx_0, \tag{3b}$$

where q is the total bunch charge per meter and x_0 and z_0 denote the location of the electrons forming the bunch at $t=0$. The bunch profile is determined by its distribution function, $f(x_0,z_0)$. Throughout this paper we assumed a longitudinal Gaussian distribution function having a full width at half maximum (FWHM) of σ_x and a δ function at the bunch height in the transverse direction. The FDTD minimum resolution was determined by $\Delta_x=\Delta_z=\sigma_x/10$ in order to support the generation of coherent radiation at wavelengths $\lambda \geqslant \sigma_x$.

A setup of the FDTD boundary conditions including the TF/SF box is shown in Fig. 2. The scattering object, which is the grating in the case of SPR, is surrounded by the TF/SF box (we found that a margin of four cells was sufficient). At each time step the TF/SF box boundaries are updated by the incident fields on its edges such that only the scattered fields escape it. The reader is referred to Ref. [17] for a detailed explanation of implementing this method. The initial bunch position should be much larger than b, thus, far enough from the grating in order to minimize the initial fields incident on the grating with respect to those when the bunch is above the grating (i.e., reduce the initial noise due to the finite running time). In our simulations an initial distance of $\sim 25b$ was used.

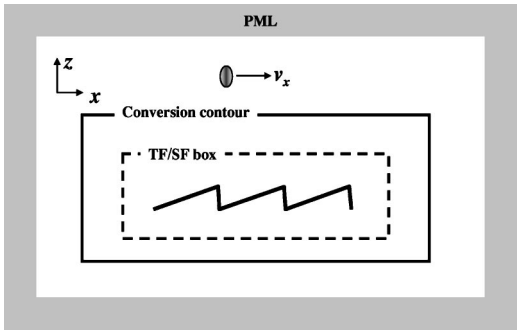

FIG. 2. FDTD setup of the boundary conditions. Total of incident and reflected fields are inside the total-field/scattered-field (TF/SF) box that contains the grating. The conversion contour for storing the data of the scattered near fields is located around the TF/SF box. The computation area is bounded by a perfectly matched layer (PML) [17].

The grating was assumed to be a perfectly conducting metal with the tangential electric component $E_{\parallel}=0$ on its edges. The grating profile was approximated by its best fit on the rectangular mesh. A perfectly matched layer (PML) [22] was used to absorb the wave propagating outside of the computation region, as shown in Fig. 2.

At each time step, $t'=n\Delta_t$, the fields on a conversion contour, $L_a(\mathbf{r}')$, are stored, where $\mathbf{r}'=\hat{x}x'+\hat{z}z'$. This contour is located outside of the TF/SF box, as shown in Fig. 2, and is used to calculate the far-field data. After the simulation ends (and the bunch is sufficiently past the grating such that the residual fields inside the computation space are negligible), a near- to far-field transformation [23] was used in order to calculate the fields at each observation point $\mathbf{r}=\hat{x}x+\hat{z}z$ and time t,

$$\mathbf{H}^{\mathrm{far}}(\mathbf{r},t) = \frac{1}{2\pi\sqrt{2r}}\int_{L_a}dl'\int_{t'=-\infty}^{t'=t-P/c}\frac{\partial_{t'}[\hat{n}_L\times\mathbf{E}(\mathbf{r}',t')]/Z_0+\partial_{t'}[\hat{n}_L\times\mathbf{H}(\mathbf{r}',t')]\times\hat{r}}{\sqrt{c(t-t')-P}}dt' \equiv \hat{y}H_y^{\mathrm{far}}, \tag{4}$$

where $P=[(x-x')^2+(z-z')^2]^{1/2}$, $\hat{n}_L$ is a unit vector normal to the conversion contour and coming out of it, and $Z_0=(\mu_0/\epsilon_0)^{1/2}$ is the free-space impedance. A Fourier transform to H_y^{far} was applied in order to find the spectral content at each observation angle and calculate the wavelength and radiated energy at the nth order.

III. EFIE FORMULATION

A. Finite-length grating

Assuming an $e^{j\omega t}$ dependence, the formulation describing the scattered TE$_y$-polarized fields from a general 2D perfectly conducting geometry is given by the electric-field integral equation solved along the perimeter of the scatterer, C [24],

$$\begin{aligned}E_{\parallel}^{\mathrm{inc}}(\mathbf{r},\omega) &= j\frac{Z_0}{k}\Bigg\{\cos\alpha\int_C J_C(\mathbf{r}',\omega)\cos\alpha'[\partial_x^2+k^2]G(\mathbf{r}-\mathbf{r}')dc' \\ &+\cos\alpha\int_C J_C(\mathbf{r}',\omega)\sin\alpha'\partial_{xz}G(\mathbf{r}-\mathbf{r}')dc' \\ &+\sin\alpha\int_C J_C(\mathbf{r}',\omega)\sin\alpha'[\partial_z^2+k^2]G(\mathbf{r}-\mathbf{r}')dc' \\ &+\sin\alpha\int_C J_C(\mathbf{r}',\omega)\cos\alpha'\partial_{xz}G(\mathbf{r}-\mathbf{r}')dc'\Bigg\},\end{aligned} \tag{5}$$

where the observation and source points on the scatterer are

$\mathbf{r}$ and $\mathbf{r}'$, respectively, the angles tangent to these points are α and α', respectively, and the 2D free-space Green's function is $G(\mathbf{r}-\mathbf{r}')=(1/4j)H_0^{(2)}(k|\mathbf{r}-\mathbf{r}'|)$. At each angular frequency $\omega=kc$, the tangential incident field at the observation point is given by the Fourier transform of Eq. (3a) for a bunch traveling above the grating,

$$E_{\parallel}^{\mathrm{inc}}(\mathbf{r},\omega)=\frac{q}{2\epsilon_0\beta c}e^{(k/\beta\gamma)z-j(k/\beta)x}\left(\frac{j\cos\alpha}{\gamma}-\sin\alpha\right)F(k), \tag{6}$$

where the bunch form factor $F(k)=\int_{x_0}\int_{z_0}e^{-(k/\beta\gamma)z_0+j(k/\beta)x_0}f(x_0,z_0)dz_0dx_0$ affects the coupling of the wake to the grating and produces the cutoff frequency due to the bunch distribution function.

The unknown Fourier harmonic of the induced surface current, $J_C(\mathbf{r}',\omega)$, in Eq. (5) was solved by dividing the grating surface into N straight segments of Δ_n length and assuming a piecewise constant current in each one,

$$J_C(\mathbf{r},\omega)\approx\sum_{n=1}^{N}a_ng_n(\mathbf{r}), \tag{7}$$

where $g_n(\mathbf{r})=1$ at the nth segment and zero out of it. Thus, Eq. (5) was approximated by a set of N linear equations $[V_m]=[Z_{mn}][I_n]$, where V_m is the incident field given by Eq. (6) at the center of the mth observation segment and $I_n=a_n$. The matrix diagonal terms, which are related to the singularity of the Hankel function, are given by the closed form [24]

$$Z_{nn}=\frac{Z_0k\Delta_n}{8}\left\{1-\frac{j}{\pi}\left[2\ln\left(\frac{1.781k\Delta_n}{4}\right)-1+\frac{16}{(k\Delta_n)^2}\right]\right\}, \tag{8}$$

and the other terms are calculated explicitly.

The far-field vector potential is found by the Hankel function approximation for a large argument $\mathbf{r}\gg\mathbf{r}'$, namely,

$$\mathbf{A}(r,\theta,\omega)\simeq-j\frac{\mu_0}{4}\sqrt{\frac{2j}{\pi kr}}e^{-jkr}\int_C J_C(\mathbf{r}',\omega)[\hat{x}\cos\alpha'+\hat{z}\sin\alpha']e^{jk(x'\sin\theta+z'\cos\theta)}dc', \tag{9}$$

and the magnetic component of the far field is [24]

$$H_y(r,\theta,\omega)\simeq-j\frac{k}{\mu_0}(A_z\sin\theta-A_x\cos\theta). \tag{10}$$

Equations (5)–(10) were computed for all frequencies up to $\omega=2\pi c/\sigma_x$ where the bunch form factor is very small. The power spectrum is given by the contribution of these frequencies at the observation angles $-\pi/2<\theta<\pi/2$,

$$P_s(\theta,\omega)=Z_0r|H_y(r,\theta,\omega)|^2, \tag{11}$$

and the angular distribution of the average radiated energy per groove per meter is given by Parseval's theorem,

$$E_{AV}(\theta)=\frac{1}{N_g\pi}\int_0^{\infty}P_s(\omega,\theta)d\omega, \tag{12}$$

where N_g is the number of grating periods. The integration range in Eq. (12) could be varied in order to calculate the energy in a specific range of frequencies for each observation angle, in order to obtain the contribution from a given SPR order, such as $0.5\omega_n<\omega<1.5\omega_n$, where $\omega_n=2\pi nc/D_g(\beta^{-1}-\sin\theta)$.

B. Periodic solution

As a step to validate the EFIE model for the finite-length grating, we have rederived Eqs. (5)–(12) for the special case of an infinitely long periodic structure. The results of this section are used in order to benchmark them to van den Berg's model [3].

In an infinitely long periodic grating, the surface current $J_C(\mathbf{r},\omega)$ takes the form $J_C(x+pD_g,z,\omega)=J_C(x,z,\omega)e^{-jk_xpD_g}$, where $k_x=k/\beta$ is the wave number in the $\hat{x}$ direction due to the bunch traveling at speed $v_x=\beta c$ above the grating. Thus, the periodic EFIE solved along a single grating period D_g will have the form [16]

$$\begin{aligned}E_{\parallel}^{\mathrm{inc}}(\mathbf{r},\omega)&=j\frac{Z_0}{k}\left\{\cos\alpha\int_{D_g}J_C(\mathbf{r}',\omega)\cos\alpha'[\partial_x^2+k^2]G_p(\mathbf{r}-\mathbf{r}')dc'\right.\\&+\cos\alpha\int_{D_g}J_C(\mathbf{r}',\omega)\sin\alpha'\partial_{xz}G_p(\mathbf{r}-\mathbf{r}')dc'\\&+\sin\alpha\int_{D_g}J_C(\mathbf{r}',\omega)\sin\alpha'[\partial_z^2+k^2]G_p(\mathbf{r}-\mathbf{r}')dc'\\&\left.+\sin\alpha\int_{D_g}J_C(\mathbf{r}',\omega)\cos\alpha'\partial_{xz}G_p(\mathbf{r}-\mathbf{r}')dc'\right\},\end{aligned} \tag{13}$$

where the 2D periodic Green's function, $G_p(\mathbf{r}-\mathbf{r}')$, replacing the free-space Green's function in Eq. (5), is

$$G_p(\mathbf{r}-\mathbf{r}')=\frac{1}{4j}\sum_{p=-\infty}^{\infty}H_0^{(2)}(k\sqrt{(x-x'-pD_g)^2+(z-z')^2})e^{-jk_xpD_g}. \tag{14}$$

The periodic surface current in Eq. (13) is found similarly, as described in the previous subsection, by dividing the single-period integration into linear segments and approximating the current as a sum of piecewise constant functions. Due to the slow convergence of the periodic Hankel function, we have used the following procedure to accelerate its evaluation [16,25]:

$$\frac{1}{4j}\sum_{p=-\infty}^{\infty} H_0^{(2)}(k\sqrt{(x-x'-pD_g)^2+(z-z')^2})e^{-jk_x pD_g}$$

$$= \frac{1}{4j}H_0^{(2)}(k\sqrt{(x-x')^2+(z-z')^2}) + \frac{e^{-jk(x-x')}}{\pi}\int_0^{\infty}\frac{\exp[-k(D_g+x-x')u^2 - j(k-k_x)D_g]\cos[k(z-z')u\sqrt{u^2+2j}]}{\{1-\exp[-kD_g u^2 - j(k-k_x)D_g]\}\sqrt{u^2+2j}}du$$

$$+ \frac{e^{jk(x-x')}}{\pi}\int_0^{\infty}\frac{\exp[-k(D_g-x+x')u^2 - j(k+k_x)D_g]\cos[k(z-z')u\sqrt{u^2+2j}]}{\{1-\exp[-kD_g u^2 - j(k+k_x)D_g]\}\sqrt{u^2+2j}}du, \quad (15)$$

where the right-hand-side first term is related to $p=0$ and the other two are related to the summation of $p=-\infty,\ldots,-1$, and $p=1,\ldots,\infty$, respectively. The advantage of this procedure is that the singularity in the self-term argument is evaluated as in Eq. (8), and the partial derivatives in Eq. (13) can be applied analytically on the second and third terms of Eq. (15).

After the periodic surface current is found, the periodic vector potential is found by [16]

$$\mathbf{A}(x,z,\omega) = \mu_0\int_{D_g} J_C(\mathbf{r}',\omega)[\hat{x}\cos\alpha' + \hat{z}\sin\alpha']G_p(\mathbf{r}-\mathbf{r}')dc'. \quad (16)$$

Applying the Poisson sum transformation over the periodic Green's function [16], we obtain

$$G_p(\mathbf{r}-\mathbf{r}') = \frac{1}{2jD_g}\sum_{n=-\infty}^{\infty}\left[\frac{e^{-jk_{xn}(x-x')-jk_{zn}|z-z'|}}{k_{zn}}\right], \quad (17)$$

where $k_{xn}=k_x+2\pi n/D_g$ and $k_{zn}=(\sqrt{k^2-k_{xn}^2})^*$ are the axial and transverse periodic wave numbers, respectively. The $()^*$ denotes a complex conjugate value; thus, $\mathrm{Re}(k_{zn})\geqslant 0$ and $\mathrm{Im}(k_{zn})\leqslant 0$. Nonevanescent radiation propagating from the grating will occur for real values of k_{zn}. These harmonics correspond to the propagating Floquet harmonics which are the spectral grating orders.

The nth SPR order is obtained from Eqs. (16) and (17) for $z>z'$,

$$\hat{y}H_{yn}(x,z,\omega) = \frac{1}{\mu_0}\nabla\times\mathbf{A} = \frac{e^{-jk_{xn}x-jk_{zn}z}}{2D_g}\int_{D_g} J_C(\mathbf{r}',\omega)[-k_{zn}\cos\alpha' + k_{xn}\sin\alpha']\frac{e^{jk_{xn}x'+jk_{zn}z'}}{k_{zn}}dc'. \quad (18)$$

It is noted that dividing this equation by the Floquet wave number dependence $e^{-jk_{xn}x-jk_{zn}z}$ results in an equation identical to Eq. (29) in [3]. The nth-order radiated energy per groove per meter is found from Eq. (18) as

$$E(\theta) = \frac{2}{\epsilon_0}|H_{yn}(\omega)|^2\frac{n\cos^2\theta}{(\beta^{-1}-\sin\theta)^2}, \quad (19)$$

where $|H_{yn}(\omega)|$ is independent of the (x,z) coordinates and ω and θ are related by the resonance condition in Eq. (1).

IV. NUMERICAL EXAMPLE

A numerical example of a finite length echelle grating by the FDTD and EFIE models is presented in the following section. The bunch and grating parameters are as listed in Table II, unless specified otherwise.

A. FDTD solution

The resulting SPR for the setup illustrated in Fig. 2 is presented in Fig. 3 by contours of H_y. Only positive contours are presented for clarity. These contours form crescent-shaped wave fronts. The 0.5-kA/m contours are located at the edges of each crescent, and incremental contours of 1.0, 1.5, and 2.0 kA/m are counted towards the interior of each crescent.

This figure was taken at a time step when the center of the bunch was at $x\simeq 25$ mm, which is just before the end of the grating. This plot provides an intuitive understanding of the SPR mechanism, in which the evanescent waves below the bunch are being reflected by the periodic structure.

It is seen that the continuation of each crescent towards large angles, $\theta\rightarrow 90°$, is tangent to the location of the bunch. These crescents end at some angle $\theta\approx 60°$ where the coherent radiation is low due to the bunch length. The number of crescents, which corresponds to the number of wave fronts

TABLE II. Smith-Purcell simulation parameters.

Bunch charge q	50 nC/m
Bunch relativistic factor γ	36
Height above the grating, $b_{\min}$	0.6 mm
Bunch length σ_x	200 μm
Grating period D_g	2.1 mm
Blaze angle α	10 degrees
Number of periods, N_g	10
Grid resolution $\Delta_x=\Delta_z$	20 μm
Stability ξ^2	0.5

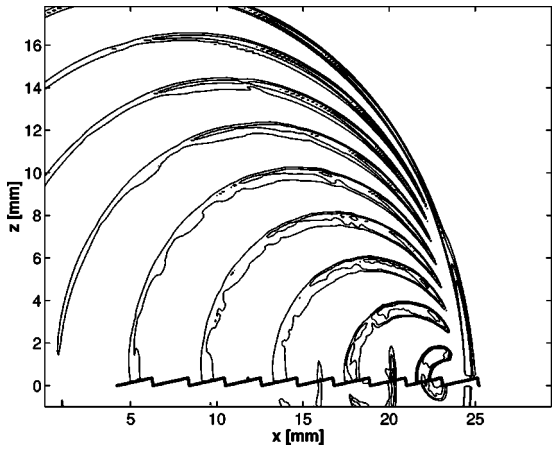

FIG. 3. A contour plot of H_y by the bunch traveling above the grating. Only positive contours of 0.5, 1.0, 1.5, and 2.0 kA/m are presented for clarity to form crescent-shaped wave fronts. The 0.5-kA/m contours are at the crescent edges and the amplitude is increasing towards the interior of each crescent.

diffracted from the grating, is equal to the number of grooves. The wavelength λ is related to the distance between two adjacent wave fronts at a given angle θ. It is noted that the computation area above $z>2$ mm was not required for the far field transformation, but was presented here for the intuitive understanding of the SPR fields.

The grating was defined as a perfectly conducting metal layer which is infinitely thin along the z dimension. In Fig. 3, electromagnetic radiation is also observed below the grating. This radiation is generated by the part of the bunch wake which passes underneath the grating and gets diffracted by the bottom of the grating. This radiation would not exist in an experiment with a finite-thickness, single-sided grating.

The far-field radiation at an observation angle of $\theta=30°$ is presented in Fig. 4. A total of ten sinusoidal periods, corresponding to the ten grating periods, are seen in this figure. The temporal distance of 3.54 ps between two adjacent peaks corresponds to a wavelength of 1.06 mm. This agrees with the theoretical wavelength at $\theta=30°$ which is 1.05 mm.

The fundamental frequency at each observation angle was computed by finding the frequency in which the Fourier

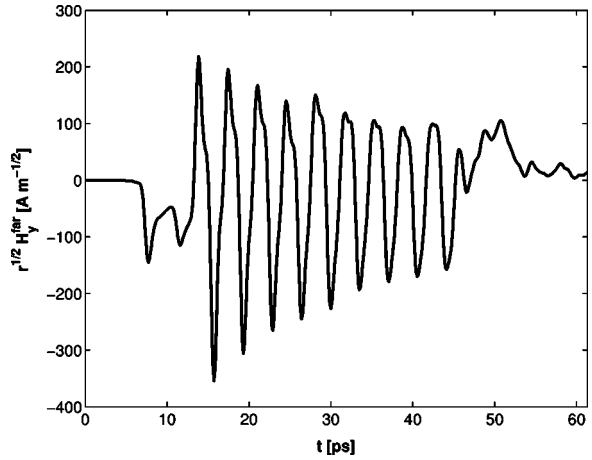

FIG. 4. Far field radiation at $\theta=30^{\circ}$.

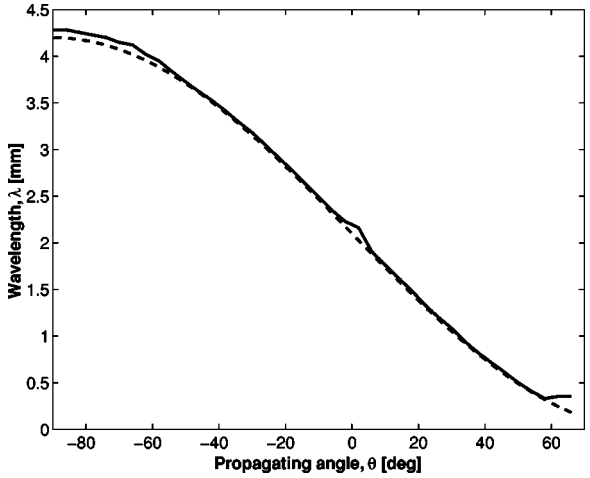

FIG. 5. Diffracted wavelength of the first-order vs propagating angle calculated from the far-field transformation (solid line) compared with the analytic result of Eq. (1) (dashed line).

transform of the far-field data is maximum. The corresponding wavelength versus θ is presented in Fig. 5 by the solid line, where the theoretical value for $n=1$ is presented by the dashed line.

B. EFIE solution

A plot of the absolute value of the surface current along the ten-period grating is presented in Fig. 6. The surface current is normalized to a unit charge of $q=1$ C/m and a bunch form factor of $F(k)=1$. The Fourier component is 285 GHz, which is related to SPR peaking at $\theta=30°$. The surface current structure has a 2.1-mm general periodicity, in agreement with the grating period, and an overall envelope which is large in the first groove and decays towards the last groove.

The surface current for an infinitely long grating, solved for the normalization and frequency settings as in Fig. 6, is presented in Fig. 7 by the solid line. The dashed line is the equivalent surface current for van den Berg's solution [Eq.

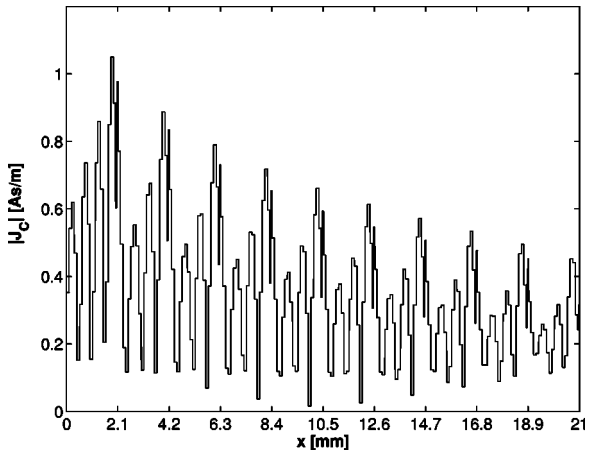

FIG. 6. Surface current at spectral frequency of 285 GHz for the ten-period grating.

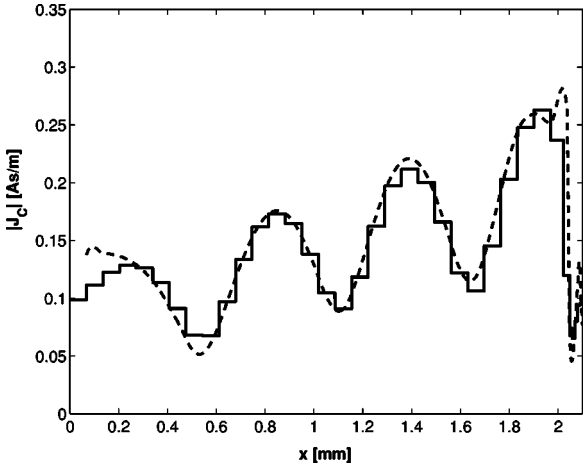

FIG. 7. Periodic surface current at spectral frequency of 285 GHz. The solid line is the periodic EFIE solution, and the dashed line is the solution of Eq. (30) in [3].

(30) in [3]]. Good agreement is obtained for the reflected fields calculated from these two solutions. This periodic surface current follows a similar structure per period as the ten-period solution in Fig. 6; however, it differs in the maximum amplitude value because it is the infinitely long grating solution, whereas Fig. 6 presents the ten-period solution. In this figure the surface current along one period (2.1 mm) has four variations. This agrees with a wavelength of 1.05 mm which corresponds to the above Fourier component.

A contour plot of the SPR power spectrum for the parameters in Table II is presented in Fig. 8. The contour values are 0.5, 1, 2, and 3×10^{-15} W s^2 (rad m)$^{-1}$. For clarity, the inner plot shows a zoomed-in section of the dashed box between 0° and 20°. The dashed curves are the first ($n=1$) and second ($n=2$) orders of the Smith-Purcell resonance in Eq. (1). It is seen that the power spectrum is located along these lines, where most of it is at the first order. The spectral width at each observation angle is $\Delta\omega/\omega\sim1/nN_g$.

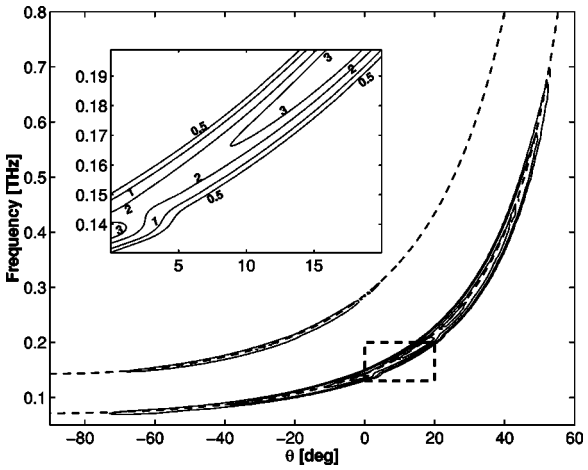

FIG. 8. Power spectrum calculated by Eq. (11). The contour values are 0.5, 1, 2, and 3×10^{-15} W s^2 (rad m)$^{-1}$. For clarity, the inner plot shows a zoomed-in section of the dashed box between 0° and 20°.

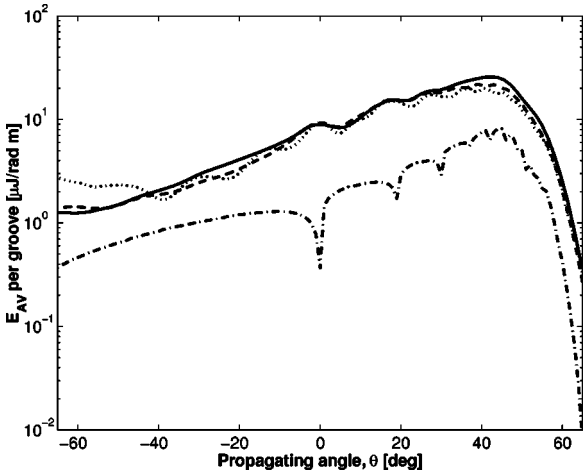

FIG. 9. Average first-order radiated energy per groove calculated by the FDTD and EFIE methods in solid and dashed lines, respectively, and the first-order energy per groove for the infinitely long grating solution in a dash-dotted line (van den Berg model). The corresponding energy for a ten-period single-sided grating having a 10 mm thickness is presented by the dotted line.

C. Radiated energy

The average first-order ($n=1$) radiated energy per groove per meter by the FDTD and EFIE models is presented in Fig. 9 by the solid and dashed lines, respectively. A good agreement with an error of ~10% is obtained between these methods. The first-order radiated energy per groove per meter by van den Berg's model, calculated at observation angle steps of 1°, is presented by the dash-dotted line.

The periodic solution deviates by a factor of more than 3 from the FDTD and EFIE solutions for the ten-period grating. Furthermore, the strong variations, related to Wood-Rayleigh anomalies [26], are not seen in the finite-length solutions.

The effect of a finite-thickness grating is presented by the dotted line. Here, the average first-order radiated energy per groove is calculated by the EFIE model for a ten-period single-sided grating (flat lower edge) having a 10 mm thickness. In Fig. 9 it is seen that a finite thickness grating hardly affects the SPR for a wide range of angles $-45°<\theta<65°$. However, diffraction radiation from the left and right edges is observed at ±90° (not shown in this figure).

The convergence of the radiated energy per groove at $\theta=25°$ for various extended grating lengths N_g to that of the infinitely long grating (van den Berg model), $\Delta E/E=(E_{AV}-E)/E$, is plotted as circles on a log-linear scale in Fig. 10, where E is the energy per groove for the infinitely long grating. In this figure, $\Delta E/E\simeq1$ for a 50-groove grating (total length of 105 mm) means it is 100% higher compared to van den Berg's solution, whereas it is only 6% higher for a 175-groove grating. The solid line represents the asymptotic convergence and its slope was found to be $e^{-0.02N_g}$.

The asymptotic convergence may be understood by the behavior of the surface current as the number of periods is increased. The amplitude of the current at the Nth groove, where $1<N\leqslant N_g$, is found to be mainly affected by the current from the preceding grooves (grooves 1 to $N-1$). For

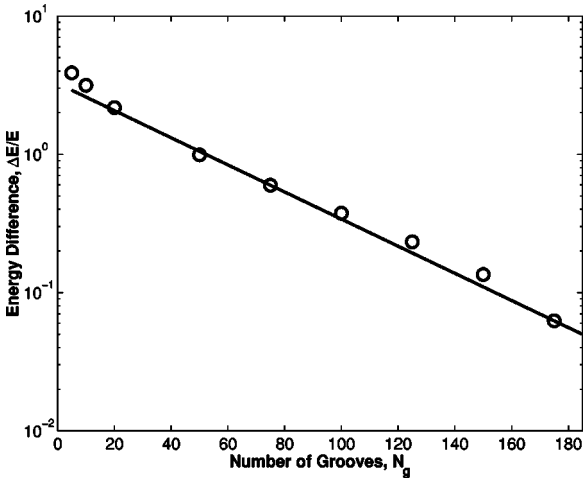

FIG. 10. Convergence of the average energy per groove calculated by the EFIE to that of the infinitely long grating (van den Berg model) at an observation angle $\theta=25°$. The circles denote the ratio $\Delta E/E$ and the solid line represents the asymptotic convergence.

example, using the parameters of Fig. 6, the Fourier harmonic of the surface current at the first groove has a peak value of ~ 1.0 As/m, independent of N_g; the peak value at the second groove is ~ 0.9 As/m for $N_g \geq 2$, etc. The solution of the surface current for a large number of periods ($N_g > 100$) follows an envelope where the amplitude approaches the periodic solution value, ~ 0.27 As/m, towards the last grooves.

V. DISCUSSION

A theoretical study of SPR by a 2D bunch above a finite-length grating was presented using two models. In the time-domain model, a TF/SF approach was used to simulate the bunch wake. The far-field signal in Fig. 4 follows an envelope which falls by a factor of 2 from the first to the last period. The same behavior is noted for the surface current at the same spectral frequency shown in Fig. 6.

The change in the surface current envelope is explained by the cumulative effects of the diffracted fields in the forward (positive x) direction. The surface current induced on the first groove, as the bunch passes above it, generates the first period of the SPR. The forward-directed part of this radiation induces current on the second groove just as the bunch is located above the second groove (for relativistic velocities), thus changing the amount of radiation from this groove. This behavior is seen in both the time- and frequency-domain solutions. For a large number of grooves, this transient settles to the periodic solution. Figure 7 shows that assuming an infinite grating length, our periodic EFIE solution agrees with the van den Berg model for the surface current.

A good agreement for the radiated energy is obtained between the FDTD and EFIE models. It is shown that van den Berg model results in a radiated energy per groove which is more than a factor of 3 lower than the average radiated energy per groove from the ten-period grating. This difference is also seen by comparing the surface current amplitude of the ten-period and the infinitely long grating in Figs. 6 and 7, respectively. The cause of this difference is the transient radiation from the initial to the successive grooves in the grating structure, as explained in the previous paragraph. Extending the grating length by increasing the number of grooves resulted in an exponential asymptotic convergence to the infinitely long solution, as shown in Fig. 10.

The edge effect due to a finite-thickness grating has a slight contribution to the SPR for angles $-45° < \theta < 65°$, as seen in Fig. 10. The left and right 10-mm edges result in coherent diffraction radiation at angles of ±90°.

The Wood-Rayleigh anomalies, predicted by the van den Berg model, have not been observed, to the best of our knowledge, in any SPR experiment. Only a mild structure in the radiated spectrum is predicted by our finite-length grating calculation.

It will be interesting to study how the SPR is affected by a realistic conductivity grating. Based on Ref. [27], we expect the same behavior for wavelengths longer than 4 μm and a significant reduction in the radiated energy for wavelengths shorter than 1 μm.

This paper extends the FDTD applications by computing the diffraction of the freespace wake by the metallic grating. It might be convenient for simulating complex grating geometries such as photonic band-gap structures [28–30] and could be used, for example, to optimize the maximum energy at a desired wavelength. Both models are limited by computer resources and required 2–3 days of computation time on a 2.65 GHz Pentium processor for the above numerical example.

ACKNOWLEDGMENTS

This research was supported by the U.S. Department of Energy, Division of High Energy Physics. A.S.K. wishes to thank Eric A. Forgy and Arthur D. Yaghjian for their helpful suggestions.

[1] S. J. Smith and E. M. Purcell, Phys. Rev. **92**, 1069 (1953).
[2] G. Toraldo Di Francia, Nuovo Cimento **16**, 61 (1960).
[3] P. M. van den Berg, J. Opt. Soc. Am. **63**, 689 (1973).
[4] P. M. van den Berg, J. Opt. Soc. Am. **63**, 1588 (1973).
[5] O. Haeberlé, P. Rullhusen, J.-M. Salomé, and N. Maene, Phys. Rev. E **49**, 3340 (1994).
[6] Yu. N. Dnestrovskii and D. P. Kostomarov, Sov. Phys. Dokl. **4**, 158 (1959).
[7] Y. Takakura and O. Haeberlé, Phys. Rev. E **61**, 4441 (2000).
[8] J. Walsh, K. Woods, and S. Yeager, Nucl. Instrum. Methods Phys. Res. A **341**, 277 (1994).
[9] J. H. Brownell, J. Walsh, and G. Doucas, Phys. Rev. E **57**,

1075 (1998).
[10] K. J. Woods, J. E. Walsh, R. E. Stoner, H. G. Kirk, and R. C. Fernow, Phys. Rev. Lett. **74**, 3808 (1995).
[11] E. L. Burdette and G. Hughes, Phys. Rev. A **14**, 1766 (1976).
[12] Y. Shibata, S. Hasebe, K. Ishi, S. Ono, M. Ikezawa, T. Nakazato, M. Oyamada, S. Urasawa, T. Takahashi, T. Matsuyama, K. Kobayashi, and Y. Fujita, Phys. Rev. E **57**, 1061 (1998).
[13] G. Doucas, M. F. Kimmitt, A. Doria, G. P. Gallerano, E. Giovenale, G. Messina, H. L. Andrews, and J. H. Brownell, Phys. Rev. ST Accel. Beams **5**, 072802 (2002).
[14] G. Doucas, M. F. Kimmitt, Th. Kormann, G. Korschinek, and C. Wallner, Int. J. Infrared Millim. Waves **24**, 829 (2003).
[15] G. Kube *et al.*, Phys. Rev. E **65**, 056501 (2002).
[16] A. F. Peterson, S. L. Ray, and R. Mittra, *Computational Methods for Electromagnetics*, IEEE/OUP Series on Electromagnetic Wave Theory (IEEE Press, New York, 1999).
[17] A. Taflove and S. C. Hagness, *Computational Electrodynamics, the Finite-Difference Time-Domain Method*, 2nd ed. (Artech House, Norwood, MA, 2000).
[18] C. Luo, M. Ibanescu, S. G. Johnson, and J. D. Joannopoulos, Science **299**, 368 (2003).
[19] A. Doria, G. P. Gallerano, E. Giovenale, G. Messina, G. Doucas, M. F. Kimmitt, H. L. Andrews, and J. H. Brownell, Nucl. Instrum. Methods Phys. Res. A **483**, 263 (2002).
[20] S. E. Korbly, A. S. Kesar, M. A. Shapiro, and R. J. Temkin, in *Proceedings of the 2003 Particle Accelerated Conference*, edited by J. Chew, P. Lucas, and S. Webber (IEEE, Piscataway, New Jersey, 2003), pp. 2536–2538.
[21] K. Yee, IEEE Trans. Antennas Propag. **14**, 302 (1966).
[22] J. P. Berenger, J. Comput. Phys. **114**, 185 (1994).
[23] S. González García, B. García Olmedo, and R. Gómez Martín, Microwave Opt. Technol. Lett. **27**, 427 (2000).
[24] C. A. Balanis, *Advanced Engineering Electromagnetics* (Wiley, New York, 1989).
[25] A. W. Mathis and A. F. Peterson, IEEE Trans. Antennas Propag. **44**, 567 (1996).
[26] *Electromagnetic Theory of Grating*, edited by R. Petit (Springer-Verlag, Berlin, 1980).
[27] C. Palmer, *Diffraction Grating Handbook*, 5th ed. (Richardson Grating Laboratory, Rochester, NY, 2002).
[28] E. I. Smirnova, C. Chen, M. A. Shapiro, J. R. Sirigiri, and R. J. Temkin, J. Appl. Phys. **91**, 960 (2002).
[29] S. Yamaguti, Jun-ichi Inoue, O. Haeberlé, and K. Ohtaka, Phys. Rev. B **66**, 195202 (2002).
[30] K. Yamamoto, R. Sakakibara, S. Yano, Y. Segawa, Y. Shibata, K. Ishi, T. Ohsaka, T. Hara, Y. Kondo, H. Miyazaki, F. Hinode, T. Matsuyama, S. Yamaguti, and K. Ohtaka, Phys. Rev. E **69**, 045601(R) (2004).